Duchenne muscular dystrophy skeletal muscle cells derived from human induced pluripotent stem cells recapitulate various calcium dysregulation pathways

Arnaud Delafenêtre [a,1], Charles-Albert Chapotte-Baldacci [a,1], Léa Dorémus [a], Emmanuelle Massouridès [b], Marianne Bernard [a], Matthieu Régnacq [a], Jérôme Piquereau [a], Aurélien Chatelier [a], Christian Cognard [a], Christian Pinset [b], Stéphane Sebille [a,*]

[a] *PRETI laboratory, University of Poitiers, France*
[b] *CECS, I-STEM, AFM, Corbeil-Essonnes, France*

ARTICLE INFO

SUMMARY

Duchenne muscular dystrophy (DMD) is an X-linked progressive muscle degenerative disease, caused by mutations in the dystrophin gene and resulting in premature death. As a major secondary event, an abnormal elevation of the intracellular calcium concentration in the dystrophin-deficient muscle contributes to disease progression in DMD. In this study, we investigated the specific functional features of induced pluripotent stem cell-derived muscle cells (hiPSC-skMCs) generated from DMD patients to regulate intracellular calcium concentration. As compared to healthy hiPSC-skMCs, DMD hiPSC-skMCs displayed specific spontaneous calcium signatures with high levels of intracellular calcium concentration. Furthermore, stimulations with electrical field or with acetylcholine perfusion induced higher calcium response in DMD hiPSC-skMCs as compared to healthy cells. Finally, Mn2+ quenching experiments demonstrated high levels of constitutive calcium entries in DMD hiPSC-skMCs as compared to healthy cells. Our findings converge on the fact that DMD hiPSC-skMCs display intracellular calcium dysregulation as demonstrated in several other models. Observed calcium disorders associated with RNAseq analysis on these DMD cells highlighted some mechanisms, such as spontaneous and activated sarcoplasmic reticulum (SR) releases or constitutive calcium entries, known to be disturbed in other dystrophin-deficient models. However, store operated calcium entries (SOCEs) were not found to be dysregulated in our DMD hiPSC-skMCs model. These results suggest that all the mechanisms of calcium impairment observed in other animal models may not be as pronounced in humans and could point to a preference for certain mechanisms that could correspond to major molecular targets for DMD therapies.

1. Introduction

Duchenne muscular dystrophy (DMD) caused by mutations in the *dystrophin* gene, is an X-linked muscle degenerative disease affecting 1.7–2.1 of 10,000 male births [1–3]. In DMD patients, the loss of dystrophin destabilizes the dystrophin glycoprotein complex (DGC), leading to sarcolemma instability and functional deficits [4]. Dystrophin also anchors dystrophin-associated proteins to the sarcolemma, including neuronal nitric oxide synthase (nNOS) [5]. The absence of functional dystrophin results in the degeneration and death of skeletal and cardiac muscles, which are subsequently replaced by fibrous tissue [6].

Currently, there is no curative treatment for DMD.

A significant secondary consequence of DMD is the abnormal elevation of intracellular calcium concentration $(Ca^{2+})_i$ in dystrophin-deficient muscles, which exacerbates disease progression. Calcium is a pivotal signaling agent in skeletal muscle cell contraction [7,8]. Maintaining Ca^{2+} concentration in skeletal muscles is crucial for continuous muscle fiber contractility [9]. Thus, Ca^{2+} ion movements in skeletal muscles involve intricate interactions among various regulated subsystems [10]. The intracellular calcium overload seen in DMD is believed to influence its pathogenesis [11], suggesting that modulating Ca^{2+} handling mechanisms might offer a promising therapeutic

approach for DMD. Studies have shown that the sarcolemma, sarcoplasmic reticulum, and mitochondria, through alteration of diverse molecular pathways, contribute to the persistent elevation of $(Ca^{2+})_i$ levels (for review, see Mareedu et al. [12]). Elevated Ca^{2+} levels activate Ca^{2+}-dependent proteases and phospholipases, causing muscle necrosis, impairing mitochondrial function, and increasing reactive oxygen species (ROS) production. These collective alterations result in muscle atrophy and contractile dysfunction.

Our current understanding of DMD pathophysiology primarily stems from studies using mouse models (mdx and its variants) that lack dystrophin and often exhibit a milder DMD phenotype [13,14]. However, these models have led to only a few therapeutic advances, highlighting the need for human-centric research models. Notably, studies investigating the role of calcium in muscle cell differentiation using human induced pluripotent stem cells (hiPSCs) are relatively scarce [11,15]. Utilizing hiPSCs in research offers a unique platform to explore muscle cell differentiation mechanisms within a human context, potentially enhancing our comprehension of muscle disorders in humans. Therefore, establishing a disease model that accurately reflects clinical symptoms or molecular pathogenesis is crucial.

Previously used Duchenne muscular dystrophy (DMD) hiPSC lines from patients with dystrophin gene mutations [16] showed two main outcomes in transcriptome and miRnome comparisons with healthy cells. First, hiPSC differentiation accurately mirrors the developmental path from mesoderm to skeletal muscle. Second, this process yields myotubes displaying DMD phenotypes [16]. Based on these insights, the current study hypothesizes that muscle cells derived from DMD patient hiPSCs may replicate the calcium dysregulation seen in DMD. Consequently, we explored the functional behaviors of both healthy and DMD hiPSC-derived muscle cells, particularly their management of intracellular calcium levels under both resting conditions and when subjected to electrical and pharmacological stimuli.

2. Material and methods

2.1. Cell cultures

2.1.1. Human induced pluripotent stem cell-derived skeletal cells

Three healthy (M180, M398, M194) and two DMD (M202 and M418) cell lines, characterized by an out-of-frame deletion of exons 8–43 for M202 and a stop codon at exon 7C for M418, have been used [16]. hiPSC-derived skeletal myoblasts were seeded and differentiated towards myotubes using commercial media (Myoblast Cell Culture Medium SKM02, Myotube Cell Culture Medium SKM03, AMSbio). Myoblasts were thawed and seeded at 8 000 cells/cm^2 in SKM02 for amplification, then seeded on glass support (glass-bottom 35 mm Petri dish, 12 mm, and 30 mm coverslips) pre-coated with carbon and coated with Matrigel (Corning) at a density of 30 000 cells/cm^2 in SKM02. After 3 days of proliferation (corresponding to myoblasts: D3), cells were cultured with the differentiation medium SKM03 for 4 days (myotube stage: D7). Experiments were performed at D3 and D7 stages.

2.1.2. Sol cell line

SolC1(−) were derived from the Sol8 cell line obtained from primary culture of normal C3H mouse soleus muscle [17]. Cells were thawed and seeded in HamF12/DMEM (1:1) medium supplemented with 10% FCS and 1% antibiotics to achieve 80% confluence. To induce differentiation, the growth medium was changed to a fusion medium (DMEM supplemented with 2% heat inactivated horse serum, insulin [10 μg/ml, Sigma-Aldrich] and 1% antibiotics). Experiments were performed at the myotube stage, 4 days after addition of fusion medium.

2.2. Intracellular calcium concentration

Intracellular calcium concentration ($[Ca^{2+}]_i$) was measured using the Fura-2-AM calcium probe (ThermoFisher Scientific). Healthy and DMD hiPSC-derived muscle cells at D3 and D7 were loaded with Fura-2AM (3 μM) for 30–45 min at 37 °C with 5% CO2. Cells were washed twice with Tyrode's solution containing 130 mM NaCl, 5.4 mM KCl, 0.8 mM MgCl$_2$, 1.8 mM CaCl$_2$, 10 mM HEPES and 5.6 mM glucose (pH 7.4). Petri dishes were mounted in the observation chamber and cells bathed in Tyrode's solution were imaged as previously described [18]. Ratiometric calcium imaging was performed with an Olympus IX73 inverted microscope (Olympus, Tokyo, France). Cells were excited at 340 and 380 nm using a Lambda 421 beam combiner (Sutter Instrument, Ballancourt-Sur-Essonne, France) and the emitted signal acquired at 510 nm using an Andor Zyla 4.2 PLUS cooled sCMOD camera (Andor Technology, Oxford Instruments, Belfast, UK). Images were acquired at 340 nm and 380 nm at a rate of 1 image/s under successively perfused solutions to obtain the minimal and maximal Fura-2 fluorescence ratios. Cells were perfused with Tyrode solution warmed at 37 °C to obtain basal calcium fluorescence. Then, Tyrode solution containing 1 mM EGTA (Sigma-Aldrich), 20 μM ionomycine (Sigma-Aldrich) and no calcium was perfused to obtain the minimum $[Ca^{2+}]_i$ and cells were then perfused with tyrode solution containing 5 mM Ca^{2+} to obtain the maximal $[Ca^{2+}]_i$. To determine basal $[Ca^{2+}]_i$, we used the Grynkiewicz equation: $[Ca^{2+}]_i=Kd*\beta*(R-Rmin/Rmax-R)$ as described previously [19].

2.3. Measurements of membrane potential

Electrophysiological studies were realized on day 3, 7 and 10 on healthy and DMD lines. Tested cells were selected by eye based on their size, their length, their cylindrical and fusiform aspect. Microelectrode measurements were carried out on monolayers of healthy and DMD hiPSC-derived myoblasts and myotubes at room temperature (≈ 21 °C). Microelectrodes (50–80 MΩ) were pulled from borosilicate glass capillaries with filaments (BF150–110–10, Sutter Instruments) using a horizontal micropipette puller (P-97, Sutter Instruments). The microelectrodes were filled with 3 M KCl and the bath solution was composed of (mM): 150 NaCl, 4 KCl, 1.1 MgCl2, 2.2 CaCl2, 10 HEPES, 5.6 glucose at pH 7.4 adjusted with NaOH solution. Microelectrode was connected to an impedance adapter (H180, Biologic, Claix, France) linked to an amplifier (VF-180, Biologic, Claix, France) and resting membrane potential (RMP) was digitalized with an analog-digital converter (Axon Digidata 1550a, Molecular Devices, San Jose, CA, USA) using pClamp software v10.2 (Molecular Devices, San Jose, CA, USA).

2.4. Spontaneous calcium fluorescence recording

For the characterization of spontaneous calcium activity of healthy and DMD hiPSC-derived myoblasts and myotubes, cells were incubated with Fluo-8AM calcium dye (5 μM, Abcam) for 15 min at room temperature in Tyrode solution (130 mM NaCl, 5.4 mM KCl, 0.8 mM MgCl$_2$, 1.8 mM CaCl$_2$, 10 mM HEPES, 5.6 mM glucose, pH 7.4). Fluo-8 fluorescence was recorded with a revolution imaging system from Andor technology featuring a spinning disk unit (CSUX1, Yokogawa, Tokyo, Japan) and an Andor Ixon+897 back illuminated EMCCD camera (16μm2 pixel size) on an Olympus inverted IX81S1F-ZDC microscope (Olympus, Tokyo, Japan). IQ3 acquisition software (Andor technology, UK) was used to acquire images of 512 × 512 pixels. Fluorescence images were visualized through an objective x20 (NA 0.75). Fluo-8 was illuminated at 488 nm with an argon laser and fluorescence emission was collected with a GFP filter set (dichroic mirror: 488 nm, emission filter: 525 nm). Recordings were performed with a x40 objective at an acquisition speed of 5 frames/s for 3 min. Fluorescence image series were extracted under ImageJ software (NIH, Bethesda, MD, USA). Fluorescence changes were expressed as fluorescence normalized to basal values (ΔF/F0). Calcium response parameters such as amplitude peak (ΔF/F0), area (U.A), duration (s), time to peak (TTP, s), recovery time (RT, s), event frequency (events/min) were calculated with a macro-software developed under the image-processing IDL 6.1 language

(Research Systems Inc., Boulder, Colorado). When the normalized fluorescence intensity exceeded 0.1 arbitrary units, calcium increases were detected. The duration (in s) corresponds to the time spent above the detection threshold. The TTP (time to peak: s) corresponds to the time required to reach the maximum fluorescence intensity, while the RT (recovery time: s) corresponds to the time required to decrease from the maximum intensity back to the threshold.

2.5. Localized calcium release analysis

2.5.1. Density of release sites

Sequences of images in fast mode were analyzed to calculate the standard deviation of the recorded fluorescence in each pixel as a function of time. During the acquisition sequence, when several releases were observed in the same location, the calculated standard deviation of pixels in this location was higher than in areas without calcium increase. Standard deviation was performed by ImageJ software to obtain one image displaying all fluorescence changes allowing to detect spontaneous localized calcium release sites [20]. Calcium release site density (10^{-3} events/μm^2) was obtained by counting the number of calcium release sites related to cell surface area.

2.5.2. Ca^{2+} release events

hiPSCs-derived myoblasts and myotubes were incubated with Fluo-8 and Ca^{2+} release events were recorded under confocal line-scanning microscope at room temperature in Tyrode solution. Fluorescent images were recorded using a FV-1000 system mounted on an Olympus IX81 inverted microscope (Olympus, Tokyo, Japan). Cells were excited with a 488 nm laser at x40 objective and two-dimensional fluorescence images were acquired in line scan mode (x, t images: 1 line/1,3 ms, line: 100 pixels) with Fluoview software (Olympus, Tokyo, Japan) and analyzed as described previously [21]. These recordings were analyzed using the HARVELE software which first allows the automated detection of signals in x, t images and then calculates morphological parameters of each detected event [22]. In brief, four parameters were determined for each Ca^{2+} release event: amplitude ($\Delta F/F0$), RT (ms), full width at half maximum (FWHM, μm), and full duration at half maximum (FDHM, ms).

2.6. Electrical field stimulation-evoked calcium activity

Healthy and DMD hiPSC-derived myoblasts and myotubes were loaded with Fluo-8 and the recordings were carried out at room temperature in Tyrode solution with the x20 objective under confocal spinning disk microscope as described previously in *Spontaneous calcium fluorescence recording* section. Electrical stimulation electrodes were placed 1 mm above the cells and were composed of 2 parallel platinum wires connected to an STM4 electrical stimulator (Bionic Instruments). A 488 nm excitation laser was used to acquire 30-second recordings at a rate of 1 frame/100 ms. After 10 s of recording, cells were stimulated with a single pulse of 1 ms at 100 mA (Video 1). The recordings were then saved in .tiff format and analyzed under ImageJ and IDL 6.1 software. For each EFS-evoked calcium release, five parameters were determined: amplitude ($\Delta F/F0$), area (A.U.), duration (s), TTP (s) and RT (s).

2.7. Pharmacological-evoked calcium activity

Healthy and DMD hiPSC-derived myoblasts and myotubes were loaded and analyzed as described previously in the previous part. 3 min were recorded at a rate of 1 frame/ 200 ms using a 488 nm excitation laser. After 20 s of recording, 100 μM of acetylcholine and 100 or 300 μM of BzATP were perfused in the dish.

2.8. Constitutive calcium entries (CCEs)

CCEs were determined by using Fura-2 quenching method as previously described [18]. In brief, healthy and DMD hiPSC-derived myoblasts and myotubes loaded with Fura-2 were bathed in Tyrode solution for 1 min before perfusing manganese solution containing (in mM): 130 NaCl, 5.4 KCl, 0.8 MgCl2, 0.5 Mn^{2+}, 10 HEPES, 5.6 glucose, pH 7.4 for 5 min. Fura-2 loaded cells were excited with a LED at 360 nm and fluorescence emission was collected at 510 nm at a frame rate of 1 image/s with Metafluor software (Molecular Devices). The fluorescence intensity quench rate (%/min) was then calculated to evaluate CCE.

2.9. Store-operated calcium entries (SOCEs)

To analyze SOCE [23], healthy and DMD hiPSC-derived myoblasts and myotubes loaded with Fura-2 were bathed in Ca^{2+} free tyrode solution with 0.2 mM EGTA. Then, thapsigargin was perfused (1 μM) to empty calcium stores from the cells, activating SOC channels. After stabilization, calcium is reintroduced in the medium with a solution of tyrode (1.8 mM of Ca^{2+}). As a positive control, ionomycin (5 μM) was perfused. Ratiometric calcium imaging was performed for intracellular calcium determination. The SOCE slope has been calculated to analyze calcium entries due to SOC channels.

2.10. Immunological staining

Cultured cells were stained with indirect immunofluorescence. Cells were rinsed with DPBS (Dulbecco's phosphate buffered saline, ThermoFisher Scientific, Massachusetts, USA) and fixed with 4 % Formaldehyde for 10 min at room temperature. Following fixation, cells were permeabilized with PBS- 0.2 % Triton X-100 for 10 min at room temperature. After washing cells with PBS, a second step of permeabilization was realized with PBS-Tween 20 at 0.1 % for 30 min at room temperature. Then, cells were probed overnight at 4 °C with anti-α-actinin (1:400, Sigma-Aldrich, Missouri, USA), and anti-myosin heavy chain (1:500, MF20, DSHB, IOWA, USA) in PBS-Tween. Cells were washed and incubated 3 h with secondary antibodies, Alexa Fluor 555 conjugated goat anti-chicken and Alexa fluor 647 donkey anti-mouse (1:500, ThermoFisher Scientific). Cells were mounted in Mowiol medium (Sigma-Aldrich). Samples were examined with a laser scanning confocal microscope (Olympus FV3000, Japan). 405 nm, 561 and 640 nm laser lines were used for excitation of DAPI (4′,6-Diamidino-2-phenylindole, Sigma-Aldrich), Alexa Fluor 555 and Alexa Fluor 647 respectively. Emission fluorescence was recorded through spectral detection channels between 430 and 470 nm (blue), 570–620 nm (red) and 650–750 nm (far red fluorescence emission). 1024 × 1024 pixels images were acquired with UPLAPO100 × 40HR objectives lens and X2 numerical zooming (0.06 μm pixel size).

2.11. Electron microscopy imaging

hiPSC-derived cells were seeded on a polycarbonate membrane (Costar 3413). After 3 days of culture (D3) and 7 days of culture (D7), cells were fixed for at least 60 min with freshly prepared 2.5 % glutaraldehyde overnight at 4 °C. After fixation, cell monolayers were washed three times in PBS and then fixed in 4 % OsO4 for 1 hour. Cells were washed again three times in PBS. The cells were then dehydrated with sequential washes in 50 %, 70 %, 90 %, 95 %, and 100 % acetone and then embedded in 50:50 mixture of acetone and Epon resin overnight. The following day specimens were placed into a fresh change of pure resin for 4 h, then embedded in another fresh change of 100 % resin, and placed in a 60 °C oven for 24 h for polymerization. The blocks were then ready for sectioning. Ultrathin sections (60-nm) with EM UC7 ultramicrotome (Leica) were collected on copper grids and stained with 2 % uranyl acetate in 50 % ethanol for 3 min, followed by incubation in lead citrate (0.08 M) for 6 min. Samples were analyzed with JEM 1010

electron microscope (Jeol) equipped with a Quemesa camera (Olympus).

2.12. Statistical analyses

P-values were calculated either by two tailed t-tests or ANOVA and completed by post-hoc tests, as indicated in the corresponding figure legends. These statistical analyses were performed using the GraphPad Prism 8 software.

3. Results

3.1. Morphology of human induced pluripotent stem cell-derived muscle cells (hiPSC-skMCs)

hiPSCs from DMD patients and healthy individuals were generated and grown as described previously [16,24]. These cells were subjected to a standardized differentiation protocol. Cells were thawed at the myoblast stage and expanded for 3 days. Myoblasts were then incubated for 4 days in a medium that induces cell differentiation (SKM03) into elongated and plurinucleated myotubes (D7). Fig. 1 describes morphology of muscle cells derived from healthy hiPSC-skMCs during amplification of myoblasts (D3) (A) and during fusion process in
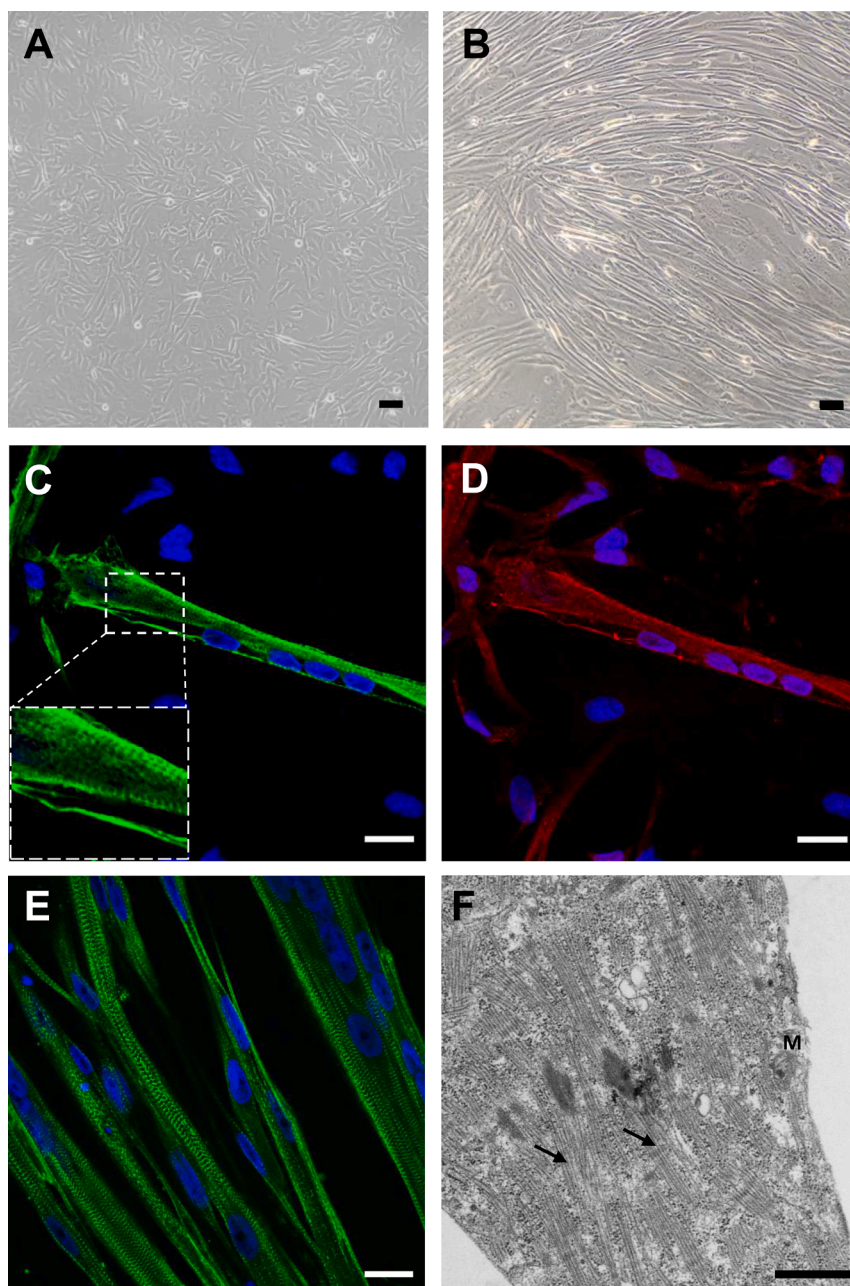
Fig. 1. Morphology and ultrastructure of human induced pluripotent stem cell-derived muscle cells (hiPSC-skMCs). A and B: Transmission images of hiPSC-derived healthy (M180) myoblasts (D3) (**A**) and after differentiation (myotubes: D7) (**B**). Scale bar: 50 μm. **C and D:** Immunostaining of healthy hiPSC-derived myotubes (D7) with α-actinin in green (**C**) and myosin heavy chain in red (**D**). Nuclei are labeled in blue (Dapi); scale bar: 20 μm. **E:** Immunostaining of DMD (M418) hiPSC-derived myotubes with α-actinin in green; scale bar: 20 μm. **F:** Electron microscopy images of hiPSC-derived myotubes (M398) (arrows indicate myosin filaments). Scale bar: 2 μm.

myotubes (D7) (B). In D7, cells were aligned and displayed elongated shapes. Fluorescent staining of nuclei and α-actinin (Fig. 1C) confirmed both the fusion in displaying several nuclei per cell and the formation of striation patterns in elongated cells. labeling of myosin heavy chains with the MF-20 antibody demonstrated their presence in striated myotubes (Fig. 1D). DMD hiPSC-skMCs myotubes also displayed α-actinin striations at the myotube stage (Fig. 1E) and electron microscopy images of such cells detected the establishment of the alignment of myosin filaments in myotubes, without striations (Fig. 1F). Both DMD and healthy myotubes could be sustained in culture for extended periods of time. However, beyond day 7, the cells exhibited pronounced contractile activity, causing them to detach from the substrate. This detachment hindered our ability to conduct most stimulation experiments.

3.2. Resting calcium levels and membrane potential values in healthy and DMD hiPSC-skMCs

Intracellular calcium concentrations ($[Ca^{2+}]_i$) have been determined, at rest, in both healthy and DMD hiPSC-skMCs lines and at both D3 and D7 stages, (Fig. 2A). Intracellular calcium concentrations were found to be close to normal values in healthy cells [25]. For DMD cells, $[Ca^{2+}]_i$ were found elevated at D3 stage. At D7 stage, no significant differences were found between healthy and DMD cells. Resting membrane potential values have also been measured with the microelectrode method in our hiPSC-skMCs cell lines at three different maturation stages (D3, D7 and D10: Fig. 2B and Figure S1). Resting membrane potential of a differentiating muscle cell allows the assessment of excitability properties and therefore its ability to activate excitation-contraction coupling mechanism. In D3 stage, cells displayed membrane potential values of -9.0 ± 1.0 mV for healthy cells and -8.1 ± 0.6 mV for DMD cells, meaning that, at this stage, cell membranes are weakly polarized (Fig. 2B), as often seen in proliferating cells. Polarization of membranes increased for both cell lines in D7 (-24.0 ± 1.9 mV for healthy cells and -19.2 ± 3.4 mV for DMD cells) and in D10 conditions (-32.8 ± 3.0 mV for healthy cells and -30.5 ± 3.7 mV for DMD cells) in which most cells formed myotubes. These findings are consistent with previous observations regarding muscle cell polarization during the maturation process [26]. Here, we can assume that hiPSC-derived muscle cells were subsequently able to generate the physiological machinery, comprising various channels and pump proteins, which facilitate ion movement across the lipid bilayer and establish negative resting potential values. No significant difference in resting membrane potential values was found between healthy and DMD cells.

### 3.3. Spontaneous calcium increases in differentiating hiPSC-skMCs

During *in vitro* maturation, skeletal muscle cells can exhibit spontaneous calcium activities, i.e. local or global calcium increase events [20, 27]. To record large and global activities, currently termed calcium oscillations, calcium imaging has been performed with confocal microscopy in DMD and healthy hiPSC-skMCs cell lines (Fig. 3A-B). Recording of spontaneous global calcium oscillations revealed multiple event profiles with varying durations and frequencies (Fig. 3B). Each of these events has been analyzed to calculate the amplitude, the frequency and three kinetic parameters (Duration, Time to Peak: TTP, and Recovery Time: RT) allowing comparison of spontaneous events in healthy and DMD cells in the two differentiation stages: myoblasts (D3) and myotubes (D7). Results showed that the amplitude of calcium events increased with cell differentiation in both cell types (Fig. 3C). Moreover, DMD cells at D7 showed a higher significant amplitude (2.99 ± 0.06) than healthy cells (2.29 ± 0.08). In terms of frequency of these events, there was no significant difference between healthy and DMD myoblasts. However, in D7 myotubes, healthy cells exhibited a significantly higher release frequency (1.55 ± 0.09 events/min) as compared to DMD myotubes (0.69 ± 0.04 events/min) (Fig. 3D). Analysis of kinetic parameters displayed a decrease in the duration of events, associated with a reduced TTP in DMD cells during differentiation from D3 to D7, with no changes in RT (Fig. 3E-G). In healthy cells, kinetic parameters showed no significant variation during differentiation (Fig. 3E-G). hiPSC-skMCs also displayed a large amount of highly localized calcium increases (Fig. 4) that were demonstrated to be mainly due to local calcium releases from sarcoplasmic reticulum in developing muscle cells [20]. These local events were recorded and analyzed through two different methods. First, release site density was calculated through the computation of the standard deviation on image series of fluo-8 loaded cells (Fig. 4A-B). Even if the number of release sites seemed not to depend on the differentiation stage in healthy cells, it was found significantly increased in DMD D7 cells (Fig. 4B). The morphology of these events has then been characterized and fluo-8 images were recorded in a line scan mode (x, t) taking fluorescence variations along a line as a function of time (Fig. 4C). The size parameter of event morphology (FWHM) (Fig. 4F) revealed a lower calcium spreading of these events in DMD cells as compared to control. Local events were also found longer along the time in DMD D7 cells as compared to healthy cells, regarding their elevated durations and RT (Fig. 4E and G respectively). All these data demonstrated that spontaneous calcium activity revealed an increase in the amount of calcium released during calcium
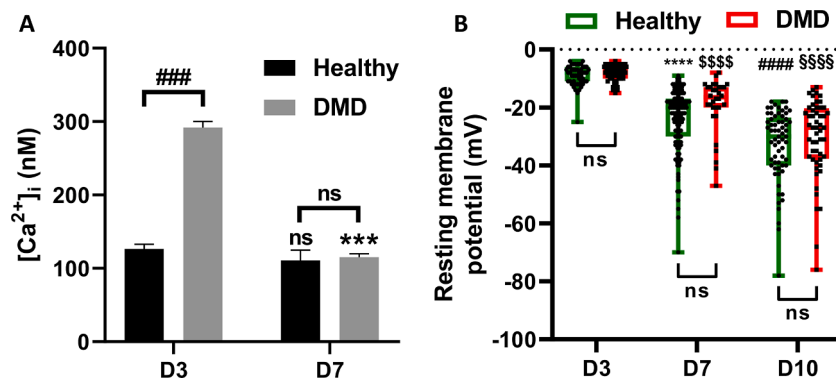
Fig. 2. Resting calcium levels and membrane potential values in healthy and DMD hiPSC-skMCs. A: Intracellular calcium concentrations determined using fura-2 dye and ratiometric method in healthy (M180) and DMD (M202) hiPSC-skMCs lines at D3 and D7. (Results shown as mean ± SEM; Healthy: D3, $n = 56$; D7, $n = 80$, $N = 4$. DMD: D3, $n = 97$; D7, $n = 92$, $N = 2$. * indicates the significant difference between D3 and D7 cells, and # between healthy and DMD. *** and ###: $p < 0.005$, Kruskal Wallis test with Dunn's multiple comparisons test). **B**: Resting membrane potential values measured with the microelectrode method in both healthy (M180 and M194) (green) and DMD (M202 and M418) (red) hiPSC-skMCs at three different maturation stages, D3, D7 and D10. (* indicates the significant difference between D3 and D7 healthy cells. # Indicates the significant difference between D7 and D10 healthy cells. $ indicates the significant difference between D3 and D7 DMD cells. § Indicates the significant difference between D7 and D10 DMD cells Healthy: D3, $n = 50$; D7, $n = 133$; D7+3, $n = 60$, $N = 6$. DMD: D3, $n = 66$; D7, $n = 32$; D7+3, $n = 52$, $N = 4$. **** and ####: $p < 0.001$, Kruskal Wallis test with Dunn's multiple comparisons test).
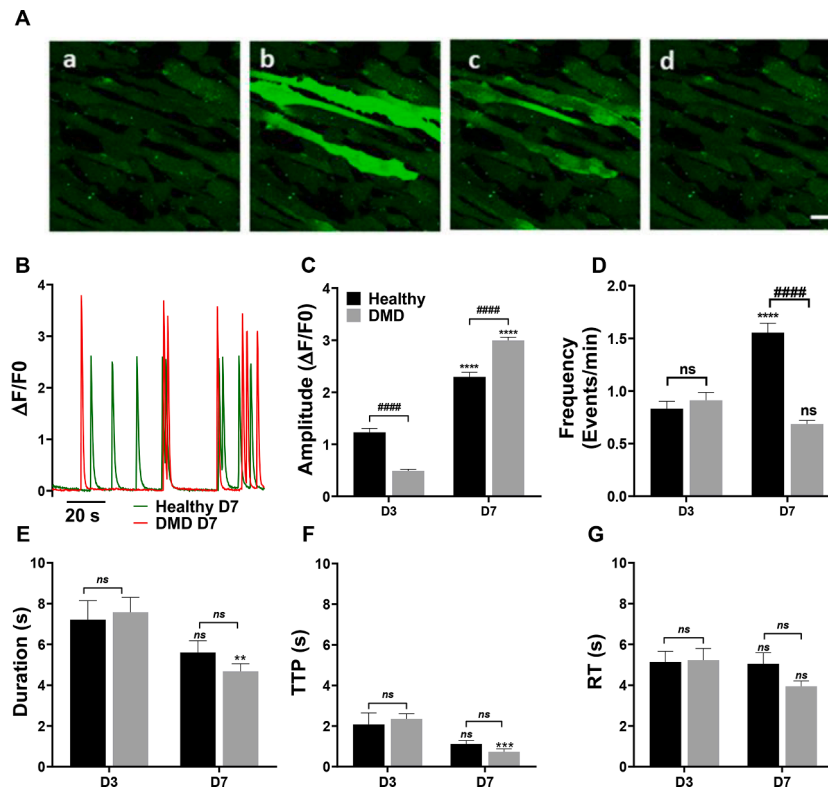
Fig. 3. Spontaneous calcium oscillations in healthy and DMD hiPSC-skMCs. A: Image series (a, b, c, d) of fluo-8 fluorescence during spontaneous calcium oscillations in healthy (M180) hiPSCs (5 fps). **B:** Examples of calcium kinetics in hiPSCs-derived myotubes in healthy (M180) and DMD (M202) cells at D7. Amplitude (**C**), Frequency (**D**), Duration (**E**), Time to peak (TTP: **F**) and Recovery time (RT: **G**) of calcium events in healthy and DMD hiPSCs-derived cells at D3 and D7. (Healthy: D3, $n = 102$; D7, $n = 275$, $N = 7$. DMD: D3, $n = 168$; D7, $n = 207$, $N = 8$. * Indicates the significant difference between D3 and D7. # indicates the significant difference between healthy and DMD lines. **: $p < 0.01$; ***: $p < 0.005$; **** and ####: $p < 0.001$, Kruskal Wallis test with Dunn's multiple comparisons test).
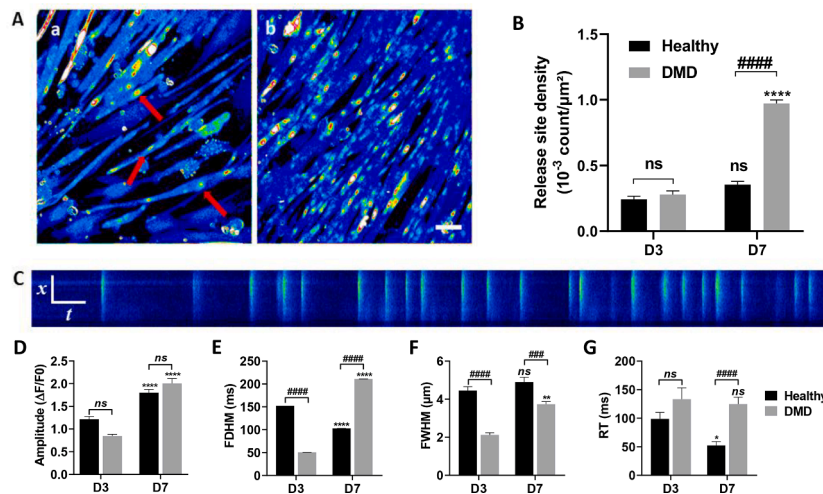
Fig. 4. Spontaneous local releases of calcium in healthy and DMD hiPSC-skMCs. A: Standard deviation images of calcium fluorescence recording (1 min) showing sites of calcium release (red arrows) identified in a culture of healthy (M180) (a) and DMD (M202) (b) hiPSC−CMs at D7. Scale bar: 20 μm. **B:** Release site density in healthy and DMD hiPSCs-derived myoblasts and myotubes (data are shown as mean ± SEM. Healthy: D3, $n = 19$; D7, $n = 20$, $N = 5$. DMD: D3, $n = 39$; D7, $n = 35$, $N = 6$. * indicates the significant difference between D3 and D7. # indicates the significant difference between healthy and DMD lines. **** and ####: $p < 0.001$, Kruskal Wallis test with Dunn's multiple comparisons test). **C:** 2-D images (800×800 pixels) acquired in a line scan mode (x, t images: 1 line/2 ms, 100 pixels) showing fluorescence variations along a line as a function of time. Amplitude (**D**) and kinetic parameters, FDHM (**E**), FWHM (**F**), and RT (**G**) (data are shown as mean ± SEM. Healthy: D3, $n = 121$; D7, $n = 264$, $N = 4$. DMD: D3, $n = 47$; D7, $n = 198$, $N = 2$. * indicates the significant difference between D3 and D7, and # between healthy and DMD. *: $p < 0.01$, **: $p < 0.005$, **** and ####: $p < 0.001$, Kruskal Wallis test with Dunn's multiple comparison test).

oscillation as differentiation progressed.

3.4. Calcium responses of hiPSC-skMCs under electrical stimulation

As it has been demonstrated that hiPSC-skMCs exhibited negative membrane potentials values, electric field stimulation (EFS) was performed on cell cultures loaded with fluo-8. Calcium increase events were recorded during EFS through calcium imaging with confocal microscopy (Fig. 5A-B and video S1). As expected, based on membrane potential values, not all cells exhibited a calcium response to this stimulation; only 20% of the myoblasts and 35% of the myotubes, regardless of cell line, displayed significant calcium elevation events. Each of these events has been analyzed to calculate amplitude (Fig. 5C), area (Fig. 5D) and three kinetic parameters (Time to Peak: TTP, Duration and Recovery Time: RT; Fig. 5E-G). Results showed that the amplitude of calcium signal increased with cell differentiation in both cell types (Fig. 5C). Moreover, DMD cells at D7 showed a higher signal than healthy cells (Fig. 5C-D) (1.42 ± 0.07 for healthy cells and 2.13 ± 0.07 for DMD cells). Analysis of kinetic parameters showed significant differences between healthy and DMD lines (Fig. 5E-G). Indeed, the duration of calcium release, the time to peak and the recovery time of myotubes (D7) were significantly higher in DMD cells as compared to healthy cells (Fig. 5E-G). Nifedipine at 1 μM completely blocked calcium increase during electrical field stimulation (Figure S2). These findings imply that calcium increase observed during electrical stimulation is mediated via DHPR channels.

3.5. Pharmacological stimulations

We were then interested in evaluating if our hiPSC-skMCs were able to respond to acetylcholine, the endogenous neurotransmitter released at the neuromuscular junction, capable of inducing skeletal muscle contraction. Acetylcholine at 100 μM was perfused on hiPSC-skMCs cultures loaded with fluo8-AM and calcium responses were determined through calcium imaging (Fig. 6A). In this case, 52 % of the myoblasts and 97 % of the myotubes, regardless of cell line, displayed significant calcium elevation events. Each of these events has been analyzed to calculate the same parameters as in Fig. 5. Results show that the amplitude of calcium signal increased with cell differentiation in both cell types (Fig. 6B-C and Figure S3). Moreover, DMD cells at D7 displayed a signal with higher amplitude (2.35 ± 0.12) as compared to healthy cells (1.90 ± 0.09). Acetylcholine perfusion was also performed using either an extracellular calcium free solution or nifedipine incubation (10 μM). These two conditions induced a significant reduction of 78 % and 73 %, respectively, in the proportion of responding cells (Fig. 6D), demonstrating the involvement of both extracellular calcium and excitation-contraction coupling elements in this acetylcholine-dependent calcium increase. Furthermore, for the few remaining responding cells, calcium signal amplitudes were found to be significantly reduced in these two inhibitory conditions. (Fig. 6E-F).

Because elevated activity of P2 × 7 receptors has been identified in myoblasts from the mdx mouse model of DMD [28], purinergic receptors have also been interrogated in our hiPSC-skMCs cultures with BzATP
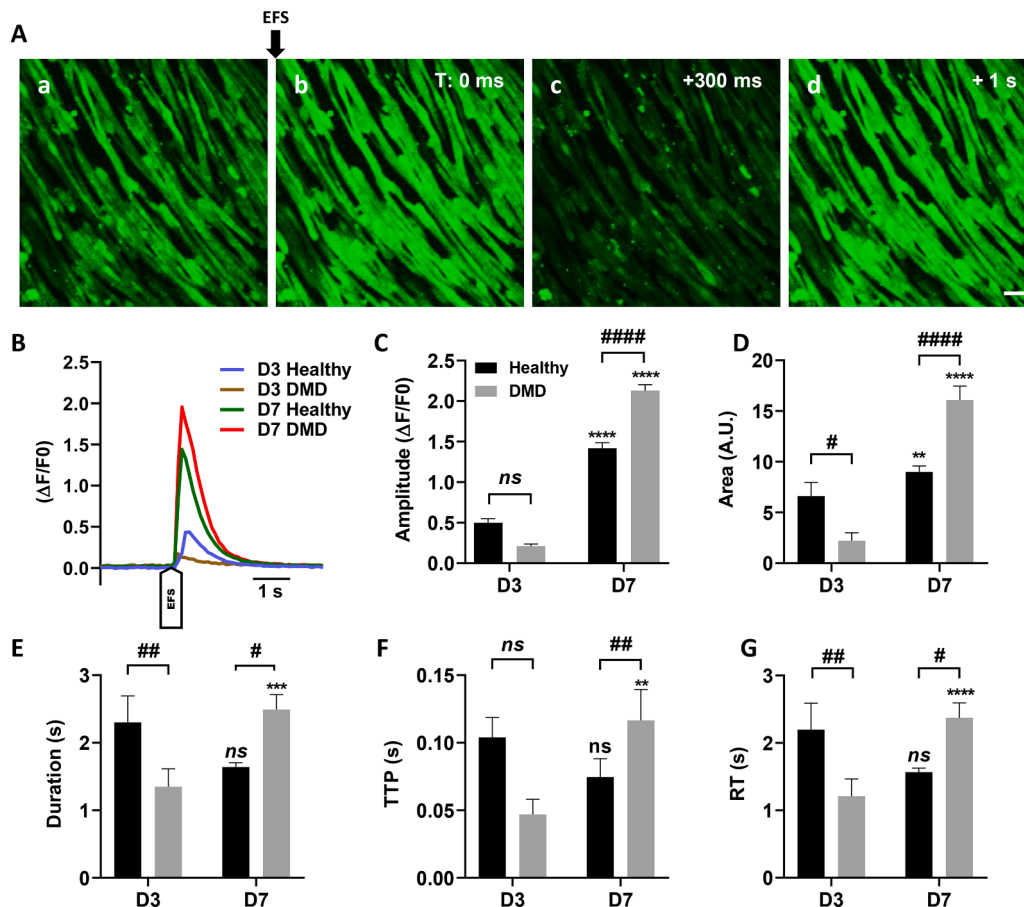
Fig. 5. Characterization of calcium responses induced by electrical field stimulation (EFS) in healthy and DMD hiPSC-skMCs. A. Representative example of fluo-8 fluorescence measurements before (a) and after (b) an EFS-induced calcium increase in healthy (M180) hiPSC—CMs. Scale bar: 20 μm. **B**: examples of kinetics obtained in each condition. Amplitude (ΔF/F0) (**C**), Area (A.U.) (**D**) as well as kinetic parameters: Duration (**E**), Time to peak (TTP) (**F**) and RT (**G**) of electrically induced calcium increases were determined in healthy (M180) and DMD (M202) hiPSC—CMs (data are shown as mean ± SEM. Healthy: D3, $n = 60$; D7, $n = 82$, $N = 11$. DMD: D3, $n = 35$; D7, $n = 133$, $N = 12$. * indicates the significant difference between D3 and D7 cells, and # between healthy and DMD. **** and ####: $p < 0.001$, Kruskal Wallis test with Dunn's multiple comparisons test).
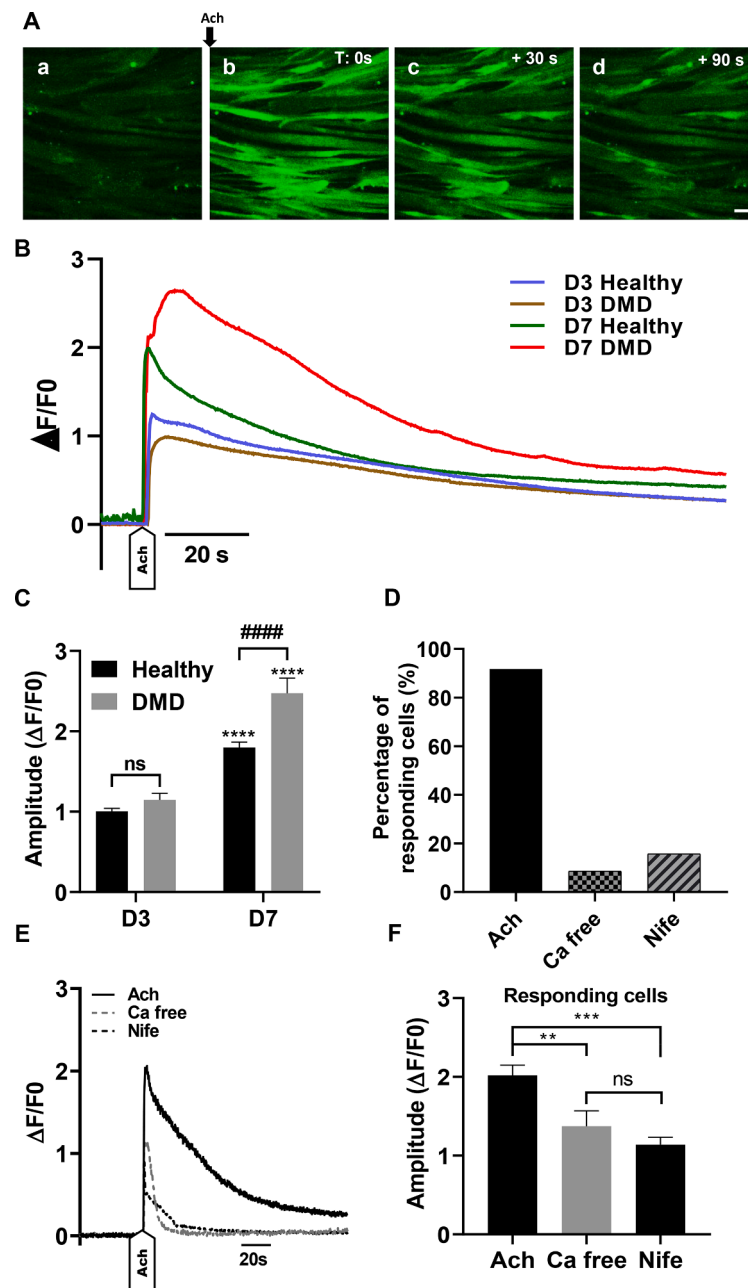
Fig. 6. Characterization of calcium responses induced by acetylcholine stimulation in healthy and DMD hiPSC-skMCs. A: Example of fluo-8 fluorescence images recorded during acetylcholine perfusion (100 μM) in healthy (M180) and DMD (M202) hiPSC—CMs. Scale bar: 20 μm **B:** Representative kinetics obtained in each condition. **C:** Analysis of the Amplitude (ΔF/F0) of acetylcholine induced calcium increases in DMD and Healthy hiPSCs. **D:** Percentage of responding cells during acetylcholine perfusion in free extracellular calcium and with nifedipine (10 μM). **E:** Kinetics obtained with Healthy hiPSCs myotubes with the amplitude (ΔF/F0) measured for each treatment (**F**). data are shown as mean ± SEM. Healthy: D3, $n = 16$; D7, $n = 16$, $N = 1$. DMD: D3, $n = 19$; D7, $n = 24$, $N = 2$. * indicates the significant difference between D3 and D7. # indicates the significant difference between healthy and DMD lines. **: $p < 0.01$, ***: $p < 0.005$, **** and ####: $p < 0.001$, Kruskal Wallis test with Dunn's multiple comparisons test.).

perfusion (100 μM and 300 μM) (Figure S4). BzATP perfusion was also performed on SolC1(-) skeletal muscle cell line, a dystrophin-deficient cell line originating from mice [20]. Results show that BzATP perfusion at 100 μM induced a large calcium increase in cultured SolC1(-) myotubes. Perfusion of BzATP with similar concentration in cultured DMD hiPSC-skMCs at D7 led to low calcium increase, which moreover involved only a small proportion of cells (around 2 % of responding cells). At a higher concentration (300 μM), both cell lines were able to respond to the stimulation (Figure S4A-B). However, responses to BzATP stimulation revealed differences between healthy and DMD cell lines. Indeed, the amplitude of calcium increase was significantly higher in

DMD cells (1.48 ± 0.23) as compared to healthy cells (0.33 ± 0.04) (Figure S4 C). Analysis of calcium kinetics in hiPSC-skMCs shows a difference between DMD cells and healthy cells, with an increased duration, TTP and RT in DMD cells (Figure S4D-E).

3.6. Constitutive and store-operated calcium entries in healthy and DMD hiPSC-skMCs

Constitutive calcium entries have been determined in both healthy and DMD hiPSC-skMCs at the same two stages D3 and D7. Such entries have been previously shown to be elevated in the context of dystrophin
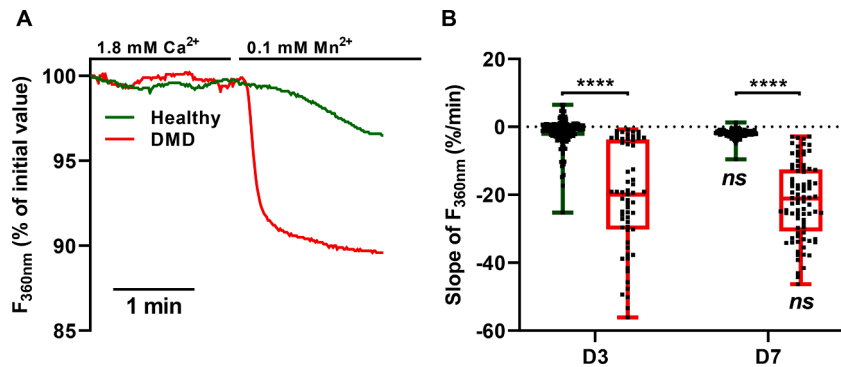
Fig. 7. Characterization of constitutive calcium entries (CCE) in healthy and DMD hiPSC-skMCs. A: Examples of CCE kinetics in hiPSC-skMCs myotubes in healthy (M180) (green) and DMD (M202) (red) conditions at D7. **B:** CCE measured in both healthy (green) and DMD (red) hiPSC-skMCs cell lines at D3 and D7. (Data are shown as mean ± SEM, healthy: D3, $n = 161$; D7 $n = 90$, $N = 2$. DMD: D3, $n = 61$; D7, $n = 84$, $N = 2$. * indicates the significant difference between D3 and D7. # indicates the significant difference between healthy and DMD lines, Kruskal Wallis test with Dunn's multiple comparisons test).

deficiency, primarily involving TRP channels [29,30]. Mn2+ quenching experiments were performed, and the rate of Fura-2 fluorescence quenching was determined as an index of calcium entry (Fig. 7). In DMD cells at D7, addition of 0.1 mM Mn2+ induced a quenching of the Fura-2 fluorescence, characterizing a constitutive entry of calcium at rest, that is not observed in healthy cells (Fig. 7A). In healthy myoblasts and myotubes, only slow constitutive calcium entries have been recorded (-1.5 ± 0.6 %/min at D3 and -1.9 ± 0.2 %/min at D7, Fig. 7B). Constitutive calcium entries were found increased in DMD cells at both stages (-21.1 ± 4.0 %/min at D3 and -21.7 ± 2.4 %/min at D7). For both cell lines, no significant differences have been calculated between D3 and D7, indicating that maturation of myoblasts into myotubes did not modify levels of constitutive calcium entries.

Store operated calcium entries (SOCEs) have also been determined in both healthy and DMD hiPSC-skMCs at the same two stages D3 and D7. SOCEs have been demonstrated to be involved in calcium dysregulation in several dystrophin deficient models [23,31]. Experimental protocols to determine SOCE have been conducted in our models (Figure S5A), using ionomycin perfusion at the end of each experiment as a positive control for calcium increase slope characterization. Results show that no significant increase in intracellular calcium, originating from SOCs, and characterized with increase slope (Figure S5B) or area (Figure S5C) was observed at D3 in both cell lines. A very low but significant increase was observed at D7 in both cell lines (Figure S5B-C). At this stage, no significant differences were found between healthy and DMD hiPSC-skMCs.

3.7. Correlation with RNA sequencing and previous studies

Given the diverse origins of calcium dysregulations, we aligned our findings with (i) previous studies that documented calcium disorder in both human and animal models, and (ii) RNA sequencing data identifying potential molecular actors of impairment with significantly altered mRNA levels in DMD compared to healthy cells [16]. We subsequently developed a scoring system: the number of studies (with human model-based studies given double weight) multiplied by the count of dysregulated transcripts (DMD vs. healthy) (Table S1). Fig. 8 presents the scoring results in a pie chart, with segments— each representing a pathway or dysregulation site—color-coded based on alignment with our findings (green: match, orange: no match, gray: undetermined). This visualization underscores pathways corroborated by our hiPSC-skMCs model data, emphasizing their role in calcium disorders in DMD, while also spotlighting areas either not universally agreed upon or warranting further investigation. Such insights could guide the identification of promising therapeutic targets for DMD treatment.
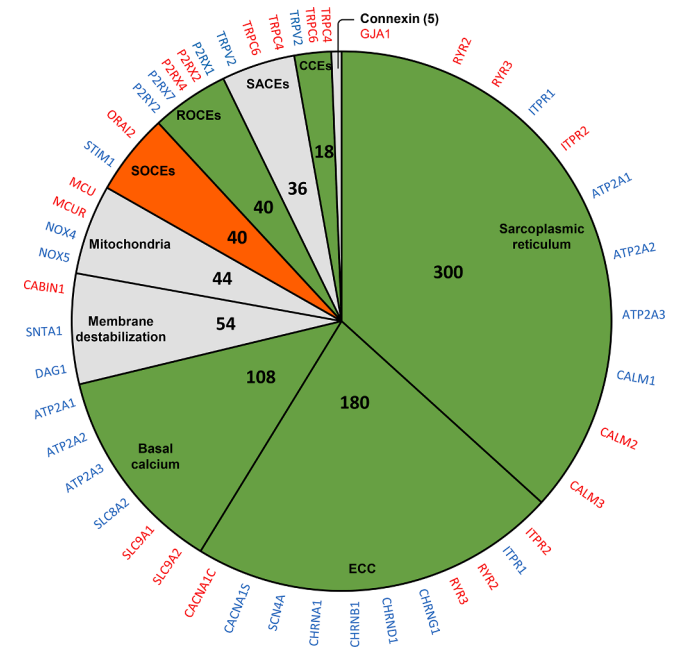
Fig. 8. mRNAs and functional deregulation observed in hiPSCs derived muscle cells at myotube stage. Pie chart depicting the various origins of calcium dysregulations in DMD. We integrated our findings with (i) previous studies that identified calcium dysregulation pathways in both human and animal models (94 publications, Table S1), and (ii) RNA sequencing results highlighting potential molecular actors of dysregulation. These actors exhibited mRNA levels that were significantly elevated or reduced in DMD compared to healthy controls [16]. We devised a scoring system based on the number of studies, with those conducted on human models given twice the weight, multiplied by the number of dysregulated transcripts (DMD vs. healthy). Each segment, representing a specific pathway or dysregulation site, is both scored and second color-coded based on its alignment with our findings: green for a match, orange for no match, and gray for undetermined. On the pie chart's outer rim, mRNAs of potentially implicated proteins that are notably under-expressed are denoted in blue, while those that are over-expressed are marked in red. Genes without discernible changes in mRNA expression are omitted from the chart [16].

4. Discussion

The primary aim of this study was to characterize the pathology in muscle cells derived from DMD patient hiPSCs (hiPSC-skMCs). This characterization involved identifying physiological changes and evaluating the cells' ability to regulate calcium concentrations at rest and

upon stimulation. We subsequently conducted a comprehensive series of tests to assess resting calcium signatures, calcium levels, elevations in calcium following electrical or pharmacological stimulation, and calcium influxes. This study primarily focused on two stages of muscle cell differentiation: the myoblast stage (D3) and the myotube stage (D7). Most of our experiments highlighted calcium dysregulation in DMD hiPSC-skMCs compared to healthy cells. However, our DMD hiPSC-skMCs models did not exhibit calcium disorder via store-operated channels.

4.1. Resting status

We investigated the resting membrane potential of hiPSC-skMCs to assess their excitability and, consequently, their contractile capacity. Our findings showed membrane potential values of -9.0 ± 1.0 mV for myoblasts, -24.0 ± 1.9 mV for myotubes, and -32.8 ± 3.0 mV for myotubes after 7 days of differentiation. In vivo studies in rats have indicated that skeletal muscle cells exhibit a more polarized membrane potential with potential values ranging between -60 and -70 mV [32]. Research on humans has reported similar resting membrane potential values, ranging from $-92 - -97$ mV [33]. Our results suggest that hiPSC-skMCs are less polarized, consistent with prior observations on cultured human cells [34], which displayed membrane potential values of -27 $\pm$ 1 mV for mononucleated myoblasts and -33 $\pm$ 2 mV for young myotubes (9 days in vitro). Despite the observed low membrane polarization, we assessed excitation-contraction coupling in our cells using both electrical stimulation and acetylcholine perfusion. Only a small proportion of myoblasts responded to either electrical stimulation or acetylcholine perfusion in both healthy and DMD cells. However, this proportion increased in myotubes, indicating a maturation process of the hiPSC-skMCs. Moreover, when nifedipine was added during acetylcholine perfusion, there was a reduction in the response of over 80% of cells (Fig. 6D). Electrical stimulation in the presence of nifedipine resulted in a complete absence of calcium increase in both cell lines (Figure S2). These findings imply that the calcium increases observed during both electrical and chemical stimulations are mediated via DHPR channels.

In skeletal muscle cells, the cytosolic calcium concentration is typically in the range of ~50–250 nM [25]. For some time, it has been recognized that calcium handling is disrupted in dystrophin-deficient cells. Specifically, intracellular calcium concentrations have been observed to be elevated in mdx mouse fibers [35], mdx myotubes [36], and in primary cultures derived from DMD patients [37]. In our study, we analyzed intracellular calcium levels to compare healthy and DMD cells derived from hiPSCs (Fig. 2A). The results indicated that the intracellular calcium level in healthy cells, both at the myoblast and myotube stages, had an approximate mean value of 120 nM. DMD myotubes did not show significant differences when compared to healthy myotubes. However, DMD myoblasts exhibited significantly elevated levels, reaching 290 nM. One potential explanation for these observations is the restoration of resting calcium homeostasis in DMD cells at the myotube stage. This restoration might be attributed to an enhanced storage capacity in hiPSC-skMCs during the myotube stage, possibly due to the maturation and fusion of myoblasts [38]. Alternatively, the elevated calcium levels might be associated with lower expression of calcium extrusion pumps (e.g., SERCAs, PMCAs) and exchangers (e.g., NCXs, NHEs) in DMD myoblasts as compared to healthy myoblasts. Furthermore, the exchangers for which transcriptional dysregulation has been identified at myoblast stage were not dysregulated in myotubes, which could explain the difference in the elevated level of intracellular calcium in DMD myoblasts. Supporting this hypothesis, our RNAseq analysis revealed decreased mRNA transcript levels for SERCA2 (DMD myoblasts: 41,907 $\pm$ 4516; DMD myotubes: 71,608 $\pm$ 5154) and NCX3 (DMD myoblasts: 335; DMD myotubes: 630) and other exchangers as NHEs as displayed in Table S1 [16].

4.2. Spontaneous calcium activities

Analysis of spontaneous calcium activity revealed an increase in the amount of calcium released during calcium oscillation throughout differentiation, consistent with observations in mdx mice [39]. It has to be noted that spontaneous calcium increases could result from fluctuations of membrane potential that have already been recorded during differentiation of human skeletal muscle cells [40]. Because our cells are not fully mature, various voltage-dependent channels (sodium and calcium channels), and even embryonic forms, can be expressed (for example, NaV1.5 in skeletal muscle cells: Table S2). Such forms can either originate from fluctuations in membrane potential or be sensitive to these fluctuations, resulting in calcium signals.

Previous research has indicated compromised intracellular calcium cycling in DMD cells [20,41]. When comparing healthy and DMD cells, we observed decreased amount of calcium released during global spontaneous calcium releases at myotube stage (Fig. 3C), aligning with studies on the *mdx* model [42]. The decrease in calcium amplitude observed in DMD myoblasts compared to healthy myoblasts can be explained by an experimental bias due to high intracellular calcium levels identified in Fig. 2A. Because of these elevated basal levels, normalization of these values with high levels of basal fluorescence leads to a reduction of amplitude values. But, despite this measurement bias, decreased calcium releases in DMD myoblasts might also be explained by IP3 receptor downregulation reflected by low levels of mRNA transcripts (Table S2). Furthermore, the frequency of calcium release events (Fig. 3) was found lower in DMD myotubes as compared to healthy myotubes. This difference could be explained by low levels of voltage dependent sodium channel (SCN) mRNA transcripts (Table S2), especially the NaV1.4 isoform (SCN4A), (Healthy myotubes: 774 $\pm$ 173; DMD myotubes: 233 $\pm$ 64; $p < 0.001$) which is predominant in skeletal muscle [43]. Then the examination of local calcium increases events in hiPSC-skMCs revealed a significant increase in the density of spontaneous calcium release in DMD cells (Fig. 4B). Moreover, the kinetics of these events differed between the two cell lines, with DMD cells exhibiting prolonged duration and rise time. An increased density of release sites could indicate a dysregulation of ryanodine receptors (RYR) [44] and/or IP3 receptors (IP3R), as we have previously shown in dystrophin-deficient muscle cell lines [20,45]. The observed kinetic differences might also be attributed to diminished SERCA expression. A reduction of SERCA activity has been documented in the mdx mouse model, underscoring the role of SERCA2a in calcium disorder in DMD [31]. Such dysregulation was also confirmed in human cells [46]. In line with these findings, reduced mRNA transcript levels were found for SERCA2 in DMD cells compared to healthy cells, as determined by RNAseq analysis, in both myoblasts (Healthy myoblasts: 70,138 $\pm$ 7142; DMD myoblasts: 41,907 $\pm$ 4516; $p < 0.01$) and myotubes (Healthy myotubes: 109,183 $\pm$ 9747; DMD myotubes: 71,608 $\pm$ 5154; $p < 0.01$) (Table S2) [16]. According to several studies, local events are mainly due to release from the sarcoplasmic reticulum (SR) [20,45] and it seems possible that simultaneous release of several local events could activate a global increase in the cell. However, in our records, such scenario has never been observed. On the other hand, extracellular calcium could participate in global spontaneous increases through the activation of channels in the sarcolemma. Therefore, the use of these two techniques to measure spontaneous calcium increases appears to be complementary. Furthermore, any of these events, local or global were found to be synchronized within individual cells.

4.3. Stimulated calcium activities

Previous studies have shown that dystrophin deficiency impacts excitation-contraction coupling (ECC) during skeletal muscle stimulation [20,47]. Our investigations using electrical stimulation revealed heightened calcium amplitude in DMD cells, suggesting potential ECC dysregulation in dystrophic cells (Fig. 5C). This finding aligns with the

observed increase in mRNA copy number for the cardiac isoform of DHPR (CACNA1C or Cav1.2) in DMD myoblasts and myotubes [16]. Overexpression of the cardiac isoform of DHPR may contribute to an altered ECC in DMD cells. However, it is important to remember that only part of the cells were able to respond to electrical stimulation. This response could be explained by the heterogeneity of the cells in our hiPSC-skMCs culture. Indeed, according to Fig. 2A, some cells exhibited a highly polarized resting membrane potential, while others had a resting membrane potential close to 0 mV. Some studies reported that a low resting membrane potential reduces the ability of cells to induce ECC with a loss of excitability [48,49] and also demonstrating the quantitative relationship between resting membrane potential, generation of action potentials, and generation of calcium transients [49]. Stimulation via acetylcholine depolarization also led to pronounced calcium amplitude in DMD cells. Notably, kinetics of calcium increases remained consistent across both cell lines. Numerous studies have corroborated our observations, showing elevated calcium responses in DMD cells compared to healthy counterparts [17,50] and others. This supports the notion of a modified calcium excitation-release coupling in DMD. Conversely, some research indicates that electrically-induced calcium release in mature dystrophic muscle fibers is lower than in healthy fibers [51–53], suggesting that calcium regulation may be improved as cells mature into muscle fibers. One theory posits that cells with severe impairment might not progress to maturity [54].

4.4. Purinergic pathways

In this study, we also investigated the activation of purinergic receptors, which are triggered by adenosine 5′-triphosphate (ATP) to facilitate the rapid flux of cations including Na^+, K^+, and Ca^{2+} [55]. Prior research on purinergic receptors has highlighted the role of P2X receptors in DMD. Specifically, muscle damage might lead to the release of extracellular ATP, which can then activate specific purinergic receptors such as P2 × 7 on immune cells, contributing to chronic inflammation [56]. Moreover, other studies showed that high concentrations of extracellular ATP induce abnormal Ca^{2+} influx in *mdx* cells [57,28]. Therefore, a purinergic pathway activator was used to determine whether the same process was involved in human model, with a DMD-affected murine skeletal muscle cell line, SolC1(-) cells, as a positive control. Perfusion of hiPSC-skMCs with BzATP, an ATP agonist, induced an increased intracellular calcium in both lines. However, calcium increases were different between healthy and DMD hiPSC-skMCs. Perfusion with BzATP led to an increased calcium influx in DMD cells as well as a dysregulation of hiPSC-skMCs calcium kinetics. The increased influx of calcium detected could be attributed to an increased number of P2 × 4 mRNA transcripts (Figure S2), which is a purinergic receptor that could be implicated in the dysregulation observed in mdx model [58]. The discrepancy between kinetics could also be attributed to diminished SERCA expression as described earlier. Collectively, these findings underscore the suitability of hiPSC-skMCs as a model for exploring calcium responses to muscle cell stimulation.

4.5. Constitutive and store-operated calcium entries

Calcium impairment has been demonstrated to be associated with heightened membrane calcium entry due to the dysregulation of TRP channels involved in CCEs, SOCEs, and SACEs (Stretch Activated Calcium Entries) [29,59–62]. SOCE represents a universal mechanism allowing Ca^{2+} to enter cells in response to a decrease in SR Ca^{2+} content [63]. In our study, both CCEs and SOCEs were analyzed in our cells to verify the dysregulation of these pathways in DMD hiPSC-derived muscle cells. Specifically focusing on CCEs, calcium entry was observed in both healthy and DMD lines. However, the amount of calcium entering the cytoplasm was greater in DMD cells compared to healthy cells (Fig. 7). This observation aligns with our RNA analysis which highlighted an overexpression of channels involved in CCEs

(specifically TRPC4 and TRPC6, Table S2) in DMD hiPSC-skMCs [16]. Yet, when analyzing store-operated calcium entry, the quantity of calcium entry through this mechanism was found to be negligible and there were no significant differences between healthy and DMD hiPSC-skMCs. This is intriguing given the pronounced differences observed in the DMD animal model [64]. Several hypotheses may explain these findings. SOCE involves various proteins such as STIM1/2, ORAI1, and TRPCs [65,66]. A closer look at mRNA expression revealed that the transcription of ORAI1, TRPC1, and STIM2 was not significantly altered in DMD cells compared to healthy cells (Table S2). However, a study on a primary culture human model indicated that, at the myotube stage, the SOCE slope was more pronounced in both healthy and DMD cells [23]. This discrepancy might relate to the model itself, potentially due to the incomplete cell maturation of hiPSC-skMCs, which might explain the absence of differences observed in the SOCE analysis for DMD cells.

4.6. Correlation with RNA sequencing and previous studies

A pie chart (Fig. 8) has been generated to visualize the alignment between three datasets: previous studies documenting calcium dysregulation in DMD, RNA sequencing data, and our experimental findings. These three datasets were found to be partly correlated and such insights could guide the identification of promising therapeutic targets for DMD treatment. The pie chart visualization underscores pathways corroborated by our hiPSC-skMCs model data, emphasizing their role in DMD calcium dysregulation. The dysfunctions observed in hiPSC-skMCs correlate with RNA sequencing data, revealing altered transcription levels of key proteins involved in the regulation of intracellular calcium (pumps, channels...). For example, an increase in mRNA copy number was found for ryanodine receptors (RyR) and P2X receptors (P2RX), and a decrease for SERCA (Table S2). However, store-operated calcium entries (SOCEs), do not show such correlation. Moreover, even if this study explored several mechanisms such as spontaneous and stimulated SR calcium releases and constitutive calcium entries, certain mechanisms were not investigated. Indeed, SACEs, mitochondrial morphology and respiration, or connexins, were also identified as dysregulated in DMD and deserve to be studied in this model in the future.

4.7. Limitations

A significant limitation of this study could be the level of differentiation of skeletal muscle cells. Indeed, myotubes upon which our study is based are young myotubes, for which we observe an immature contractile apparatus and a weak cell polarization compared to mature muscles [67]. This maturation level, even if it allows the identification of differences between healthy and DMD cell lines, could explain the lack of responses to activation of SOCEs.

RNA sequencing does not provide information on the quantity of proteins produced, which is a significant limitation for the study of therapeutic targets only by RNAseq. It would also be interesting to carry out a proteomic study that could provide new information.

It would be valuable to produce an isogenic line to confirm that the absence of dystrophin induces calcium dysregulation and that the variations observed are not caused by the cell line, thus excluding genetic bias. Nevertheless, the cells used in this study have been demonstrated to show similar specific phenotypes and recapitulate key aspects of DMD pathology when compared to control cells [16]. Furthermore, the M202 DMD harbors a large out-of-frame deletion (Deletion exons 8–43) in the DMD, which would be impossible to correct even with CRISPR editing.

5. Conclusion

In summary, our data strongly suggest that DMD hiPSC-skMCs exhibit intracellular calcium dysregulation, consistent with observations in various other models. Our findings, supported by RNAseq analyses, spotlight several mechanisms known to be disrupted in other

dystrophin-deficient models. However, store-operated calcium entry mechanisms, were not found to be dysregulated in our DMD hiPSC-skMCs model. This could suggest that the disorders observed in animal models might not be as prominent in human models. It is conceivable that in a more differentiated model, dysregulations considered as non-significant in our study might become evident. Nonetheless, we believe that DMD hiPSC-skMCs serve as a valuable model for studying calcium dysregulation in Duchenne Muscular Dystrophy. These cells would be highly valuable for molecular screening studies. The large quantity of cells produced, combined with cell normalization, could facilitate the investigation of drug effects in the pathology. Indeed, three major dysregulations were highlighted in this DMD model: exacerbated calcium increases following stimulation of the SR, reduced calcium re-uptake capacities, and exacerbated CCEs. Identifying a molecule that can mitigate one of these impairments could greatly benefit patients. Furthermore, these cells could also be considered for combined therapy approach. Gene therapy is widely used to attempt to express dystrophin. However, this may not be sufficient on its own. Therefore, a combined approach involving both gene therapy and drug therapy could be a promising strategy for treating DMD [68].

Contributors

A.D. performed experiments, analyzed the data, and wrote the manuscript. C-A. C-B. performed experiments, analyzed the data and revised the manuscript. L.D. performed electron microscopy experiments. E.M. provided protocols for hiPSC-skMCs culture, provided expert support and revised the manuscript. M.B., M.R. and J.P. provided expert support to the project. (investigation). A.C. and C.C. designed the electrophysiological approach. C.P. provided expert support to the project and revised the manuscript. S.S. conceived and coordinated the project, analyzed the data, wrote the manuscript and secured funding.

CRediT authorship contribution statement

Arnaud Delafenêtre: Writing – original draft, Investigation, Formal analysis. **Charles-Albert Chapotte-Baldacci:** Methodology, Investigation. **Léa Dorémus:** Methodology, Investigation. **Emmanuelle Massouridès:** . **Marianne Bernard:** Validation, Methodology. **Matthieu Régnacq:** Validation, Resources, Methodology. **Jérôme Piquereau:** Validation, Methodology. **Aurélien Chatelier:** Resources. **Christian Cognard:** Resources, Methodology, Conceptualization. **Christian Pinset:** Validation, Resources, Conceptualization. **Stéphane Sebille:** Writing – review & editing, Writing – original draft, Supervision, Software, Project administration, Conceptualization.

Declaration of competing interest

The authors declare that they have no known competing financial interests or personal relationships that could have appeared to influence the work reported in this paper.

Data availability

Data will be made available on request.

Acknowledgments

Supplementary materials

Supplementary material associated with this article can be found, in the online version, at doi:10.1016/j.ceca.2024.102943.

References

[1] E.P. Hoffman, R.H. Brown, L.M. Kunkel, Dystrophin: the protein product of the duchenne muscular dystrophy locus, Cell 51 (1987) 919–928, https://doi.org/10.1016/0092-8674(87)90579-4.

[2] M.J. Parsons, I. Campos, E.M.A. Hirst, D.L. Stemple, Removal of dystroglycan causes severe muscular dystrophy in zebrafish embryos, Dev. Camb. Engl. 129 (2002) 3505–3512, https://doi.org/10.1242/dev.129.14.3505.

[3] J. Dooley, K.E. Gordon, L. Dodds, J. MacSween, Duchenne muscular dystrophy: a 30-year population-based incidence study, Clin. Pediatr. (Phila.) 49 (2010) 177–179, https://doi.org/10.1177/0009922809347777.

[4] D.P. Millay, S.A. Goonasekera, M.A. Sargent, M. Maillet, B.J. Aronow, J. D. Molkentin, Calcium influx is sufficient to induce muscular dystrophy through a TRPC-dependent mechanism, Proc. Natl. Acad. Sci. U. S. A. 106 (2009) 19023–19028, https://doi.org/10.1073/pnas.0906591106.

[5] J.E. Brenman, D.S. Chao, S.H. Gee, A.W. McGee, S.E. Craven, D.R. Santillano, Z. Wu, F. Huang, H. Xia, M.F. Peters, S.C. Froehner, D.S. Bredt, Interaction of nitric oxide synthase with the postsynaptic density protein PSD-95 and alpha1-syntrophin mediated by PDZ domains, Cell 84 (1996) 757–767, https://doi.org/10.1016/s0092-8674(00)81053-3.

[6] I. Desguerre, M. Mayer, F. Leturcq, J.-P. Barbet, R.K. Gherardi, C. Christov, Endomysial fibrosis in duchenne muscular dystrophy: a marker of poor outcome associated with macrophage alternative activation, J. Neuropathol. Exp. Neurol. 68 (2009) 762–773, https://doi.org/10.1097/NEN.0b013e3181aa31c2.

[7] S. Ebashi, Calcium ions and muscle contraction, Nature 240 (1972) 217–218, https://doi.org/10.1038/240217a0.

[8] A.G. Szent-Györgyi, Calcium regulation of muscle contraction, Biophys. J. 15 (1975) 707–723, https://doi.org/10.1016/S0006-3495(75)85849-8.

[9] M.K. Tu, J.B. Levin, A.M. Hamilton, L.N. Borodinsky, Calcium signaling in skeletal muscle development, maintenance and regeneration, Cell Calcium 59 (2016) 91–97, https://doi.org/10.1016/j.ceca.2016.02.005.

[10] R. Bravo-Sagua, P. V, M.-C. F, S.-A. P, G. V, C.-F. A, C. M, L. S, Sarcoplasmic reticulum and calcium signaling in muscle cells: Homeostasis and disease, Int. Rev. Cell Mol. Biol. (2020) 350, https://doi.org/10.1016/bs.ircmb.2019.12.007.

[11] T. Uchimura, T. Asano, T. Nakata, A. Hotta, H. Sakurai, A muscle fatigue-like contractile decline was recapitulated using skeletal myotubes from Duchenne muscular dystrophy patient-derived iPSCs, Cell Rep. Med. 2 (2021) 100298, https://doi.org/10.1016/j.xcrm.2021.100298.

[12] S. Mareedu, R. Pachon, J. Thilagavathi, N. Fefelova, R. Balakrishnan, N. Niranjan, L.-H. Xie, G.J. Babu, Sarcolipin haploinsufficiency prevents dystrophic cardiomyopathy in mdx mice, Am. J. Physiol. Heart Circ. Physiol. 320 (2021) H200–H210, https://doi.org/10.1152/ajpheart.00601.2020.

[13] J.W. McGreevy, C.H. Hakim, M.A. McIntosh, D. Duan, Animal models of Duchenne muscular dystrophy: From basic mechanisms to gene therapy, Dis. Model. Mech. 8 (2015) 195–213, https://doi.org/10.1242/dmm.018424.

[14] W.D. Coley, L. Bogdanik, M.C. Vila, Q. Yu, J.H. Van Der Meulen, S. Rayavarapu, J. S. Novak, M. Nearing, J.L. Quinn, A. Saunders, C. Dolan, W. Andrews, C. Lammert, A. Austin, T.A. Partridge, G.A. Cox, C. Lutz, K. Nagaraju, Effect of genetic background on the dystrophic phenotype in mdx mice, Hum. Mol. Genet. 25 (2016) 130–145, https://doi.org/10.1093/hmg/ddv460.

[15] E. Shoji, H. Sakurai, T. Nishino, T. Nakahata, T. Heike, T. Awaya, N. Fujii, Y. Manabe, M. Matsuo, A. Sehara-Fujisawa, Early pathogenesis of Duchenne muscular dystrophy modelled in patient-derived human induced pluripotent stem cells, Sci. Rep. 5 (2015) 12831, https://doi.org/10.1038/srep12831.

[16] V. Mournetas, E. Massouridès, J.-B. Dupont, E. Kornobis, H. Polvèche, M. Jarrige, A.R.L. Dorval, M.R.F. Gosselin, A. Manousopoulou, S.D. Garbis, D.C. Górecki, C. Pinset, Myogenesis modelled by human pluripotent stem cells: A multi-omic study of Duchenne myopathy early onset, J. Cachexia Sarcopenia Muscle 12 (2021) 209–232, https://doi.org/10.1002/jcsm.12665.

[17] E. Marchand, B. Constantin, H. Balghi, M.-C. Claudepierre, A. Cantereau, C. Magaud, A. Mouzou, G. Raymond, C. Braun, C. Cognard, Improvement of calcium handling and changes in calcium-release properties after mini- or full-length dystrophin forced expression in cultured skeletal myotubes, Exp. Cell Res. 297 (2004) 363–379, https://doi.org/10.1016/j.yexcr.2004.02.032.

[18] C.-A. Chapotte-Baldacci, G. Lizot, C. Jajkiewicz, M. Lévêque, A. Penna, C. Magaud, V. Thoreau, P. Bois, S. Sebille, A. Chatelier, Fine tuning of calcium constitutive entry by optogenetically-controlled membrane polarization: Impact on cell migration, Cells 9 (2020) 1684, https://doi.org/10.3390/cells9071684.

[19] G. Grynkiewicz, M. Poenie, R.Y. Tsien, A new generation of Ca2+ indicators with greatly improved fluorescence properties, J. Biol. Chem. 260 (1985) 3440–3450.

[20] H. Balghi, S. Sebille, L. Mondin, A. Cantereau, B. Constantin, G. Raymond, C. Cognard, Mini-dystrophin expression down-regulates IP3-mediated calcium release events in resting dystrophin-deficient muscle cells, J. Gen. Physiol. 128 (2006) 219–230, https://doi.org/10.1085/jgp.200609559.

[21] C. Lorin, M. Gueffier, P. Bois, J.-F. Faivre, C. Cognard, S. Sebille, Ultrastructural and functional alterations of EC coupling elements in mdx cardiomyocytes: an analysis from membrane surface to depth, Cell Biochem. Biophys. 66 (2013) 723–736, https://doi.org/10.1007/s12013-013-9517-8.

[22] S. Sebille, A. Cantereau, C. Vandebrouck, H. Balghi, B. Constantin, G. Raymond, C. Cognard, Calcium sparks in muscle cells: interactive procedures for automatic detection and measurements on line-scan confocal images series, Comput. Methods Programs Biomed. 77 (2005) 57–70, https://doi.org/10.1016/j. cmpb.2004.06.004.

[23] R. Harisseh, A. Chatelier, C. Magaud, N. Déliot, B. Constantin, Involvement of TRPV2 and SOCE in calcium influx disorder in DMD primary human myotubes with a specific contribution of α1-syntrophin and PLC/PKC in SOCE regulation, Am. J. Physiol. Cell Physiol. 304 (2013) C881–C894, https://doi.org/10.1152/ ajpcell.00182.2012.

[24] E. Massouridès, J. Polentes, P.-E. Mangeot, V. Mournetas, J. Nectoux, N. Deburgrave, P. Nusbaum, F. Leturcq, L. Popplewell, G. Dickson, N. Wein, K. M. Flanigan, M. Peschanski, J. Chelly, C. Pinset, Dp412e: A novel human embryonic dystrophin isoform induced by BMP4 in early differentiated cells, Skelet. Muscle 5 (2015) 40, https://doi.org/10.1186/s13395-015-0062-6.

[25] S. Gehlert, W. Bloch, F. Suhr, Ca2+-dependent regulations and signaling in skeletal muscle: from electro-mechanical coupling to adaptation, Int. J. Mol. Sci. (2015) 16, https://doi.org/10.3390/ijms16011066.

[26] C. Fennelly, S. Soker, Bioelectric properties of myogenic progenitor cells, Bioelectricity. 1 (2019) 35–45, https://doi.org/10.1089/bioe.2018.0002.

[27] C.-A. Chapotte-Baldacci, C. Cognard, P. Bois, A. Chatelier, S. Sebille, Handling a mature calcium signature through optogenetics improves the differentiation of primary murine myotubes, Cell Calcium 103 (2022) 102546, https://doi.org/ 10.1016/j.ceca.2022.102546.

[28] J. Róg, A. Oksiejuk, D.C. Górecki, K. Zabłocki, Primary mouse myoblast metabotropic purinoceptor profiles and calcium signalling differ with their muscle origin and are altered in mdx dystrophinopathy, Sci. Rep. 13 (2023) 9333, https:// doi.org/10.1038/s41598-023-36545-y.

[29] J. Sabourin, C. Cognard, B. Constantin, Regulation by scaffolding proteins of canonical transient receptor potential channels in striated muscle, J. Muscle Res. Cell Motil. 30 (2009) 289–297, https://doi.org/10.1007/s10974-010-9206-9.

[30] E. Aguettaz, J.J. Lopez, A. Krzesiak, L. Lipskaia, S. Adnot, R.J. Hajjar, C. Cognard, B. Constantin, S. Sebille, Axial stretch-dependent cation entry in dystrophic cardiomyopathy: Involvement of several TRPs channels, Cell Calcium 59 (2016) 145–155, https://doi.org/10.1016/j.ceca.2016.01.001.

[31] S.A. Goonasekera, C.K. Lam, D.P. Millay, M.A. Sargent, R.J. Hajjar, E.G. Kranias, J. D. Molkentin, Mitigation of muscular dystrophy in mice by SERCA overexpression in skeletal muscle, J. Clin. Invest. 121 (2011) 1044–1052, https://doi.org/ 10.1172/JCI43844.

[32] O. Tyapkina, E. Volkov, L. Nurullin, B. Shenkman, I. Kozlovskaya, E. Nikolsky, F. Vyskocil, Resting membrane potential and Na+,K+-ATPase of rat fast and slow muscles during modeling of hypogravity, Physiol. Res. 58 (2009) 599–603, https:// doi.org/10.33549/physiolres.931810.

[33] R.L. Ruff, D. Whittlesey, Na+ current densities and voltage dependence in human intercostal muscle fibres, J. Physiol. 458 (1992) 85–97, https://doi.org/10.1113/ jphysiol.1992.sp019407.

[34] S.T. Iannaccone, K.-X. Li, N. Sperelakis, Transmembrane electrical characteristics of cultured human skeletal muscle cells, J. Cell. Physiol. 133 (1987) 409–413, https://doi.org/10.1002/jcp.1041330230.

[35] P.R. Turner, T. Westwood, C.M. Regen, R.A. Steinhardt, Increased protein degradation results from elevated free calcium levels found in muscle from mdx mice, Nature 335 (1988) 735–738, https://doi.org/10.1038/335735a0.

[36] F.W. Hopf, P.R. Turner, W.F. Denetclaw, P. Reddy, R.A. Steinhardt, A critical evaluation of resting intracellular free calcium regulation in dystrophic mdx muscle, Am. J. Physiol. 271 (1996) C1325–C1339, https://doi.org/10.1152/ ajpcell.1996.271.4.C1325.

[37] N. Imbert, C. Cognard, G. Duport, C. Guillou, G. Raymond, Abnormal calcium homeostasis in duchenne muscular dystrophy myotubes contracting in vitro, Cell Calcium 18 (1995) 177–186, https://doi.org/10.1016/0143-4160(95)90062-4.

[38] E.B. Ezerman, H. Ishikawa, Differentiation of the sarcoplasmic reticulum and T system in developing chick skeletal muscle in vitro, J. Cell Biol. 35 (1967) 405–420, https://doi.org/10.1083/jcb.35.2.405.

[39] N.R. Campbell, S.P. Podugu, M.B. Ferrari, Spatiotemporal characterization of short versus long duration calcium transients in embryonic muscle and their role in myofibrillogenesis, Dev. Biol. 292 (2006) 253–264, https://doi.org/10.1016/j. ydbio.2005.11.040.

[40] N. Imbert, C. Vandebrouck, G. Duport, G. Raymond, A.A. Hassoni, B. Constantin, M.J. Cullen, C. Cognard, Calcium currents and transients in co-cultured contracting normal and Duchenne muscular dystrophy human myotubes, J. Physiol. 534 (2001) 343–355, https://doi.org/10.1111/j.1469-7793.2001.00343.x.

[41] M. DiFranco, C.E. Woods, J. Capote, J.L. Vergara, Dystrophic skeletal muscle fibers display alterations at the level of calcium microdomains, Proc. Natl. Acad. Sci. U. S. A. 105 (2008) 14698–14703, https://doi.org/10.1073/pnas.0802217105.

[42] A.R. Burr, J.D. Molkentin, Genetic evidence in the mouse solidifies the calcium hypothesis of myofiber death in muscular dystrophy, Cell Death. Differ. 22 (2015) 1402–1412, https://doi.org/10.1038/cdd.2015.65.

[43] S.C. Cannon, Sodium Channelopathies of Skeletal Muscle, Handb. Exp. Pharmacol. 246 (2018) 309–330, https://doi.org/10.1007/164_2017_52.

[44] S. Pouvreau, L. Royer, J. Yi, G. Brum, G. Meissner, E. Ríos, J. Zhou, Ca(2+) sparks operated by membrane depolarization require isoform 3 ryanodine receptor channels in skeletal muscle, Proc. Natl. Acad. Sci. U. S. A. 104 (2007) 5235–5240, https://doi.org/10.1073/pnas.0700748104.

[45] L. Mondin, H. Balghi, B. Constantin, C. Cognard, S. Sebille, Negative modulation of inositol 1,4,5-trisphosphate type 1 receptor expression prevents dystrophin-deficient muscle cells death, Am. J. Physiol. Cell Physiol. 297 (2009) C1133–C1145, https://doi.org/10.1152/ajpcell.00048.2009.

[46] N.B. Wasala, Y. Yue, W. Lostal, L.P. Wasala, N. Niranjan, R.J. Hajjar, G.J. Babu, D. Duan, Single SERCA2a Therapy ameliorated dilated cardiomyopathy for 18 months in a mouse model of duchenne muscular dystrophy, Mol. Ther. J. Am. Soc. Gene Ther. 28 (2020) 845–854, https://doi.org/10.1016/j.ymthe.2019.12.011.

[47] O. Friedrich, M. Both, J.M. Gillis, J.S. Chamberlain, R.H.A. Fink, Mini-dystrophin restores L-type calcium currents in skeletal muscle of transgenic mdx mice, J. Physiol. 555 (2004) 251–265, https://doi.org/10.1113/jphysiol.2003.054213.

[48] F. Lehmann-Horn, K. Jurkat-Rott, R. Rüdel, Diagnostics and therapy of muscle channelopathies, Guidelines of the Ulm Muscle Centre, Acta Myol. 27 (3) (2008) 98–113.

[49] X. Wang, M. Nawaz, C. DuPont, J.H. Myers, S.R. Burke, R.A. Bannister, B.D. Foy, A. A. Voss, M.M. Rich, The role of action potential changes in depolarization-induced failure of excitation contraction coupling in mouse skeletal muscle, Elife 11 (2022) e71588, https://doi.org/10.7554/eLife.71588.

[50] C. Cognard, B. Constantin, M. Rivet-Bastide, G. Raymond, Intracellular calcium transients induced by different kinds of stimulus during myogenesis of rat skeletal muscle cells studied by laser cytofluorimetry with Indo-1, Cell Calcium 14 (1993) 333–348, https://doi.org/10.1016/0143-4160(93)90054-a.

[51] C.E. Woods, D. Novo, M. DiFranco, J.L. Vergara, The action potential-evoked sarcoplasmic reticulum calcium release is impaired in mdx mouse muscle fibres, J. Physiol. 557 (2004) 59–75, https://doi.org/10.1113/jphysiol.2004.061291.

[52] C.E. Woods, D. Novo, M. DiFranco, J. Capote, J.L. Vergara, Propagation in the transverse tubular system and voltage dependence of calcium release in normal and mdx mouse muscle fibres, J. Physiol. 568 (2005) 867–880, https://doi.org/ 10.1113/jphysiol.2005.089318.

[53] E.O. Hernández-Ochoa, S.J.P. Pratt, R.M. Lovering, M.F. Schneider, Critical role of intracellular RyR1 calcium release channels in skeletal muscle function and disease, Front. Physiol. 6 (2015) 420, https://doi.org/10.3389/fphys.2015.00420.

[54] F. De Backer, C. Vandebrouck, P. Gailly, J.M. Gillis, Long-term study of Ca2+ homeostasis and of survival in collagenase-isolated muscle fibres from normal and mdx mice, J. Physiol. 542 (2002) 855–865, https://doi.org/10.1113/ jphysiol.2002.020487.

[55] R.A. North, Molecular physiology of P2X receptors, Physiol. Rev. 82 (2002) 1013–1067, https://doi.org/10.1152/physrev.00015.2002.

[56] D.C. Górecki, P2X7 purinoceptor as a therapeutic target in muscular dystrophies, Curr. Opin. Pharmacol. 47 (2019) 40–45, https://doi.org/10.1016/j. coph.2019.02.003.

[57] C.N.J. Young, D.C. Górecki, P2RX7 Purinoceptor as a therapeutic target-the second coming? Front. Chem. 6 (2018) 248, https://doi.org/10.3389/fchem.2018.00248.

[58] D. Yeung, K. Zabłocki, C. Lien, T. Jiang, S. Arkle, W. Brutkowski, J. Brown, H. Lochmuller, J. Simon, E.A. Barnard, D.C. Górecki, Increased susceptibility to ATP via alteration of P2X receptor function in dystrophic mdx mouse muscle cells, FASEB J. 20 (2006) 610–620, https://doi.org/10.1096/fj.05-4022com.

[59] C. Vandebrouck, D. Martin, M. Colson-Van Schoor, H. Debaix, P. Gailly, Involvement of TRPC in the abnormal calcium influx observed in dystrophic (mdx) mouse skeletal muscle fibers, J. Cell Biol. 158 (2002) 1089–1096, https://doi.org/ 10.1083/jcb.200203091.

[60] A. Vandebrouck, T. Ducret, O. Basset, S. Sebille, G. Raymond, U. Ruegg, P. Gailly, C. Cognard, B. Constantin, Regulation of store-operated calcium entries and mitochondrial uptake by minidystrophin expression in cultured myotubes, FASEB J. 20 (2006) 136–138, https://doi.org/10.1096/fj.04-3633fje.

[61] A. Vandebrouck, J. Sabourin, J. Rivet, H. Balghi, S. Sebille, A. Kitzis, G. Raymond, C. Cognard, N. Bourmeyster, B. Constantin, Regulation of capacitative calcium entries by alpha1-syntrophin: association of TRPC1 with dystrophin complex and the PDZ domain of alpha1-syntrophin, FASEB J. Off. Publ. Fed. Am. Soc. Exp. Biol. 21 (2007) 608–617, https://doi.org/10.1096/fj.06-6683com.

[62] P. Gailly, TRP channels in normal and dystrophic skeletal muscle, Curr. Opin. Pharmacol. 12 (2012) 326–334, https://doi.org/10.1016/j.coph.2012.01.018.

[63] J.W. Putney, A model for receptor-regulated calcium entry, Cell Calcium 7 (1986) 1–12, https://doi.org/10.1016/0143-4160(86)90026-6.

[64] M. Onopiuk, W. Brutkowski, C. Young, E. Krasowska, J. Róg, M. Ritso, S. Wojciechowska, S. Arkle, K. Zabłocki, D.C. Górecki, Store-operated calcium entry contributes to abnormal Ca2+ signalling in dystrophic mdx mouse myoblasts, Arch. Biochem. Biophys. 569 (2015) 1–9, https://doi.org/10.1016/j. abb.2015.01.025.

[65] B. Darbellay, S. Arnaudeau, S. König, H. Jousset, C. Bader, N. Demaurex, L. Bernheim, STIM1- and Orai1-dependent store-operated calcium entry regulates human myoblast differentiation, J. Biol. Chem. 284 (2009) 5370–5380, https:// doi.org/10.1074/jbc.M806726200.

[66] B. Darbellay, S. Arnaudeau, D. Ceroni, C.R. Bader, S. Konig, L. Bernheim, Human muscle economy myoblast differentiation and excitation-contraction coupling use the same molecular partners, STIM1 and STIM2, J. Biol. Chem. 285 (2010) 22437–22447, https://doi.org/10.1074/jbc.M110.118984.

[67] R.L. Ruff, D. Whittlesey, Na+ current densities and voltage dependence in human intercostal muscle fibres, J. Physiol. 458 (1992) 85–97.

[68] G. Cordova, E. Negroni, C. Cabello-Verrugio, V. Mouly, C. Trollet, Combined therapies for duchenne muscular dystrophy to optimize treatment efficacy, Front. Genet. 9 (2018) 114, https://doi.org/10.3389/fgene.2018.00114.